

Contents lists available at ScienceDirect

Petroleum Science

journal homepage: www.keaipublishing.com/en/journals/petroleum-science



Original Paper

Dynamic simulation of double-cased perforation in deepwater high temperature and high-pressure oil and gas wells



Gang Bi ^{a, b, *}, Fei Han ^b, Jie-Min Wu ^b, Pei-Jie Yuan ^b, Shuai-Shuai Fu ^b, Ying Ma ^b

- a Shaanxi Key Laboratory of Well Stability and Fluid & Rock Mechanics in Oil and Gas Reservoirs, Xi'an Shiyou University, Xi'an, 710065, Shaanxi, China
- ^b College of Petroleum Engineering, Xi'an Shiyou University, Xi'an, 710065, Shaanxi, China

ARTICLE INFO

Article history: Received 27 October 2023 Received in revised form 13 May 2024 Accepted 13 May 2024 Available online 15 May 2024

Edited by Jia-Jia Fei

Keywords:
Deepwater HTHP
Double-cased perforation
Optimization of perforation parameters
Dynamic simulation
Full-scale perforation simulation

ABSTRACT

In order to ensure the penetrability of double-cased perforation in offshore oil and gas fields and to maximize the capacity of perforation completion, This study establishes a dynamic model of double-cased perforation using ANSYS/LS-DYNA simulation technology. The combination of critical perforation parameters for double casing is obtained by studying the influencing factors of the jet-forming process, perforation depth, diameter, and stress changes of the inner and outer casing. The single-target perforation experiments under high-temperature and high-pressure (HTHP) conditions and ground full-scale ring target perforation tests are designed to verify the accuracy of numerical simulation results. The reduced factor is adopted as the quantitative measure of perforation depth and diameter for different types of perforation charge under different conditions. The results show that the perforation depth reduction increases with temperature and pressure, and the reduced factor is between 0.67 and 0.87 under HTHP conditions of 130 °C/44 MPa and 137 °C/60 MPa. Comparing the results of the numerical simulation and the full-scale test correction, the maximum error is less than 8.91%, and this numerical simulation has strong reliability. This research provides a basis for a reasonable range of double-cased perforation parameters and their optimal selection.

© 2024 The Authors. Publishing services by Elsevier B.V. on behalf of KeAi Communications Co. Ltd. This is an open access article under the CC BY license (http://creativecommons.org/licenses/by/4.0/).

1. Introduction

The South China Sea has huge oil and gas reserves, with the main oil and gas resources located in deepwater, accounting for 70% of its total oil and gas resources. Deepwater oil and gas resources are the main area of exploration and development in the South China Sea. Deepwater oil and gas resources are mostly located in high-temperature and high-pressure formations, and the directional wells drilled are deepwater HTHP oil and gas wells, making drilling and completion operations extremely difficult. To ensure well wellbore stability and a high recovery ratio, some oil and gas wells are completed by double-cased perforation, but double-cased perforation technology is rarely used in China, and there is a lack of relevant theory and technology, so it is significant to research the optimal design and analysis of double-cased perforation parameters for deepwater HTHP oil and gas wells (Zhao et al., 2021; Kong et al., 2017).

E-mail address: big@xsyu.edu.cn (G. Bi).

The optimization of conventional perforation parameters focuses on the selection of perforation depth, perforation diameter, perforation density, and phase angle. The objective is to select perforation parameters that achieve the maximum capacity ratio with minimum damage to the casing and oil layer (Luo et al., 2015; Hu et al., 2014). Chen et al. (2018) used the horizontal well perforation completion productivity prediction model and the casing strength loss calculation model for thermal recovery wells after perforation as the theoretical basis, the casing strength loss as a safety criterion, and the maximum capacity ratio as the target, combined with orthogonal tests, to optimize the conventional perforation parameters for offshore heavy oil wells. Li et al. (2019) and Wang et al. (2018) modified the plane flow effect skin of perforation skin under the premise of considering the effect of flow friction in the perforation tunnel, and performed parameter sensitivity analysis based on the modified perforation skin calculation formula to form a new method for optimal perforation parameter optimization design. Dou et al. (2016) addressed the problem of large internal and external pressure differences in the casing of high-pressure fractured wells, which are prone to burst or torn along perforations. Based on the ANSYS finite element analysis method, they analyzed the effect of perforation density, perforation diameter, and phase angle variation on the burst strength of the

^{*} Corresponding author. Shaanxi Key Laboratory of Well Stability and Fluid & Rock Mechanics in Oil and Gas Reservoirs, Xi'an Shiyou University, Xi'an, 710065, Shaanxi, China.

perforated casing under the combined effect of external pressure, internal pressure, and axial force to optimize the best perforation parameters. Deng et al. (2019) used LS-DYNA to establish the propagation attenuation model of perforation impact load, fitted a computational model to predict the impact load at different locations of the tubing interval, and proposed an optimization measure for perforation in ultra-deep wells based on casing stability. Liu et al. (2022) used ANSYS/LS-DYNA software to study the impact damage of metal jets on the casing and proposed a new method of designing and optimizing perforation parameters for the casing stress distribution law between the perforation holes. Wang et al. (2022) investigated the effects of the horizontal stress difference and engineering factors such as the injection rate, number of clusters, perforation diameter, perforation length, and perforation density on the near-wellbore fracture morphology, cluster efficiency, and injection pressure during oriented limited-entry perforation and helical perforation through three-dimensional experimental and numerical investigations of perforation fracturing, and designed the perforation parameters accordingly. Dong et al. (2021) established a three-dimensional numerical model of spiral perforation hydraulic fracture propagation in near wellbore horizontal wells based on the basic equations of fluid-structure coupling and the cohesive fracture model to study the effect of perforation parameters during volume fracturing of horizontal wells in shale reservoirs and to optimize the design. The above research routinely starts from basic theories such as perforation skin calculations and combines with methods such as finite elements to do an optimal evaluation of the perforation scheme while satisfying the objectives and constraints, from which the optimal combination of perforation parameters is found (Xing et al., 2022).

Based on the above-mentioned research on the optimization of conventional cased perforation completion parameters, we will carry out special research on deepwater HTHP well conditions and double-cased perforation penetrability and safety. The novelties of this paper are in the use of ANSYS/LS-DYNA to establish numerical simulation of two types of high-temperature perforation charge with deep penetration and a big hole to penetrate the double-layer casing, to analyze the jet energy attenuation, the influencing factors of the perforation depth and perforation diameter, and the strength load of the inner and outer casing, and to propose a critical combination of perforation parameters in the context of guaranteeing the penetrability and safety of the double-layer casing perforation. The innovative combination of HTHP working conditions and double-layer casing perforation test is designed to simulate the reservoir HTHP environment of the double-layer casing perforation experiment. The goal is to establish the quantitative relationship between the depth and diameter of different types of perforation charge under different temperature and pressure conditions. The test results under the actual formation temperature and pressure conditions are used to verify the accuracy of the numerical simulation results, and an optimization scheme for perforation parameters is proposed. In conclusion, this study provides data support and a theoretical basis for the optimization of perforation parameters of the offshore HTHP double-layer casing perforation completion process and the optimization of casing performance evaluation.

2. Dynamic simulation of double-cased perforation in deepwater HTHP oil and gas wells

2.1. Dynamic simulation of double-cased perforation

In this paper, ANSYS software, Solid164, is selected to model the solid units of perforation charge, perforation fluid, inner and outer casing, inner and outer cement sheath, and reservoir to construct a

dynamic simulation model of double-cased perforation. We chose the Lagrange constant stress solid element algorithm to calculate the casing, cement layer, and perforation steel case. The algorithm can effectively simulate structural deformation and stress changes such as the collapse of the shaped charge cover under the explosive blast and the jet penetration into the casing. The ALE multi-material element algorithm is selected to calculate the explosive, shaped charge cover, and perforation fluid. The algorithm enables fluid-solid coupling, which allows the explosive and other materials to flow arbitrarily in the grid for the simulation of jet formation, impact propagation, and the effect of blast load on the structure (Hu et al., 2017).

As shown in the double casing model in Fig. 1(a), the specifications of the two-layer casing are set concerning the P110 steel grade, with a casing density of 7.8 g/cm³, an elastic modulus of 205 GPa and a Poisson's ratio of 0.3; the outer diameter of the inner casing is 177.8 mm and the wall thickness is 11.51 mm; the outer casing has an outside diameter of 244.5 mm and a wall thickness of 13.84 mm. The specifications of the cement ring are set concerning concrete material, the wall thickness of the sandwich cement sheath is 19.51 mm; the thickness of the outer cement sheath is 56.66 mm, the density is 2.3 g/cm³, the modulus of elasticity is 12.3 GPa, and the Poisson's ratio is 0.18. Stratum thickness set at 1000 mm, material density of 2.2 g/cm³, modulus of elasticity of 24 GPa, Poisson's ratio of 0.25.

As shown in the perforation charge model in Fig. 1(b), the meshing order is copper liner, explosive materials, and perforation steel case, where the explosive materials and copper liner are ALE cell meshes and steel case is Lagrange cell mesh. The material of the copper liner is purple copper with a density of 7.96 g/cm³.

As shown in the meshing model in Fig. 1, considering that the mesh sparsity is related to the accuracy of simulation and computational speed, we encrypted the local mesh at the metal particle perforation, including perforating charge mesh, casing mesh, and fluid mesh.

The temperature and pressure boundary conditions are set as shown in Fig. 2, and the dynamic simulation of the perforation process of charge explosion is subsequently carried out.

Referring to the stress distribution in different cells at the same moment during the explosion of the copper liner, the formation, development, and impact intrusion of the shaped charge jet into the double casing are shown in Fig. 3. The changes in dynamic loading during perforation are studied, and the results of this simulation are used as the basis for the evaluation study of the perforation effect.

Taking 78.76 μ s as an example, as shown in Fig. 3(a), the metal particle flow has penetrated the inner casing, and the inner casing has failed; the stress has gradually decreased; and the high-stress area has shown a dispersion. Throughout the penetration process, the high-stress area shows a circular shape; as in Fig. 3(b), the inner cement ring is completely penetrated, the high-stress area disappears, and the stress in the ring area gradually decreases; as in Fig. 3(c), the metal particle flow starts to contact the outer casing, when the stress concentration area gradually expands with a circular distribution; as in Fig. 3(d), with the action of metal particle flow on the outer casing, the maximum stress dissipates around the center of perforation, at which point a portion of the stress is transferred to the outer cement ring.

2.2. Analysis of factors influencing double-cased perforation parameters

Based on the dynamic simulation of the deep double-cased perforation process, the following parameters were selected: High-temperature explosive (HMX), hole density 16–60 shots/m,

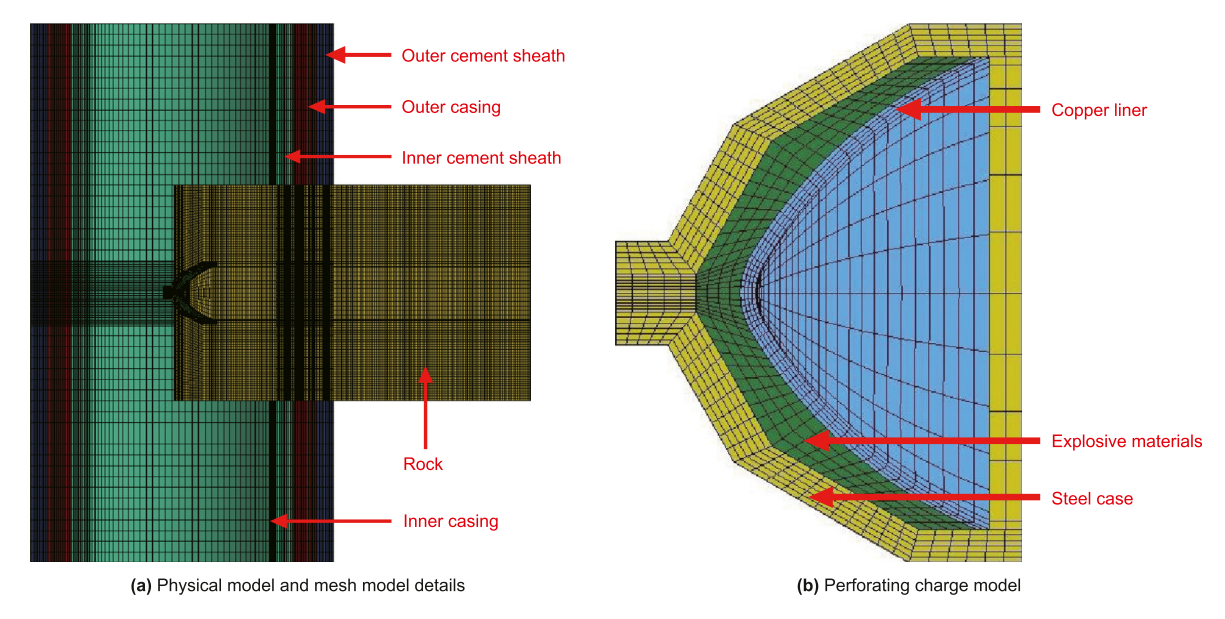


Fig. 1. Double-cased perforation geometric model.

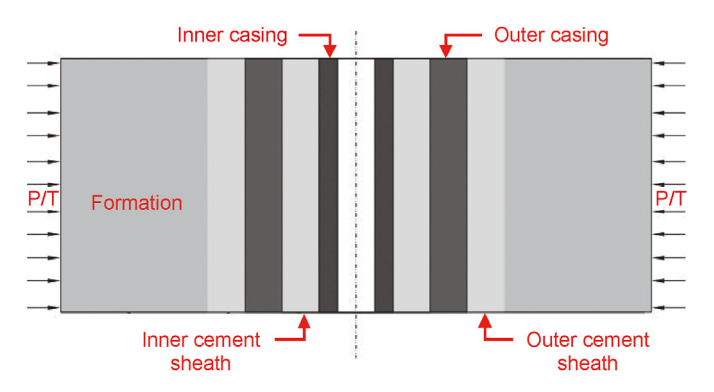


Fig. 2. Setting of boundary conditions of numerical simulation calculation model.

phase angle $0-180^\circ$, TCP positive pressure perforation method, to study the relationship between the perforation parameters of deep penetrating (DP) and big hole perforation charge (BH) and jet velocity, inner and outer casing perforation diameter and perforation depth, inner and outer casing strength, etc.

The structure of the DP perforation charge is shown in Fig. 4(a), with the front end of the copper liner tapered at an angle of 45° , the outer diameter of the steel case 44 mm, the diameter of the copper liner 38 mm, the wall thickness of the copper liner 1.6 mm, and the charge height 29 mm.

The structure of the BH perforation charge is shown in Fig. 4(b). The front end of the copper liner is rounded, the angle is 120° , the outer diameter of the steel case is 57 mm, the diameter of the copper liner is 50 mm, the wall thickness of the copper liner is 1.65 mm, and the charge height is 34.5 mm.

According to the simulation results of different perforation charges penetrating the double casing, it can be concluded that the maximum-shaped charge jet velocity generated by the explosion of perforation charges shows a positive correlation with the charge mass, as shown in Fig. 5(a). Compared with DP charges, BH charges have a larger charge cover flare angle and a smaller gathering energy effect, so at the same charge, the maximum velocity of BH charges is smaller.

Failure criteria for the casing and reservoir are defined, and the

length and width of the hole formed by model failure are the perforation depth and diameter as the polygonal jet forms and penetrates. With the increase in charge mass, the perforation diameter gradually increases. As shown in Fig. 5(b), for the DP charge, when the charge mass is 25 g, the velocity of the shaped charge jet is 8940 m/s, the perforation depth is 430 mm, and the perforation diameter is 8.35 mm. When the charge mass is 25 g, the velocity is 8240 m/s, the perforation depth is 340 mm, and the perforation diameter is 11.28 mm. Under the same charge mass, the perforation depth caused by a BH charge is smaller than that caused by a DP charge, and the diameter is larger.

Under simulated actual working conditions, the formation limits of penetration for DP charges and BH charges with different charge masses are studied, as shown in Fig. 6. The velocity of shaped charge jets all shows a decaying trend and can be roughly divided into stages such as penetration of the inner casing, the cement layer, the outer casing, and punching through the casing.

According to the combination of the double casing, considering the requirements of penetration depth and perforation diameter, when the charge mass >25 g and the initial velocity exceeds 8000 m/s, it can ensure that the velocity of the perforation charge leaving the outer casing >850 m/s and the penetration distance of the DP charge also exceeds 400 mm. The critical conditions for the penetration of double-cased perforation are established.

During the perforation operation, the perforation diameter and density will affect the extrusion strength of the casing to different degrees. With the increase in external load, the external extrusion force on the casing after perforation increases, and the maximum extrusion stress generated by the casing increases. When the external load reaches a certain value, the maximum extrusion stress produced by the casing after perforation reaches the maximum yield strength of the casing, and the external extrusion force on the casing at this time is the net extrusion strength to meet the yield strength requirement of the casing after perforation. The casing sections with different perforation densities and diameters are selected separately to analyze their effects on the yield strength of the casing after perforation and to determine the net extrusion strength to meet the casing yield strength requirements.

Referring to the relationship between perforation diameter, perforation density, and residual collapsing strength of casing, the

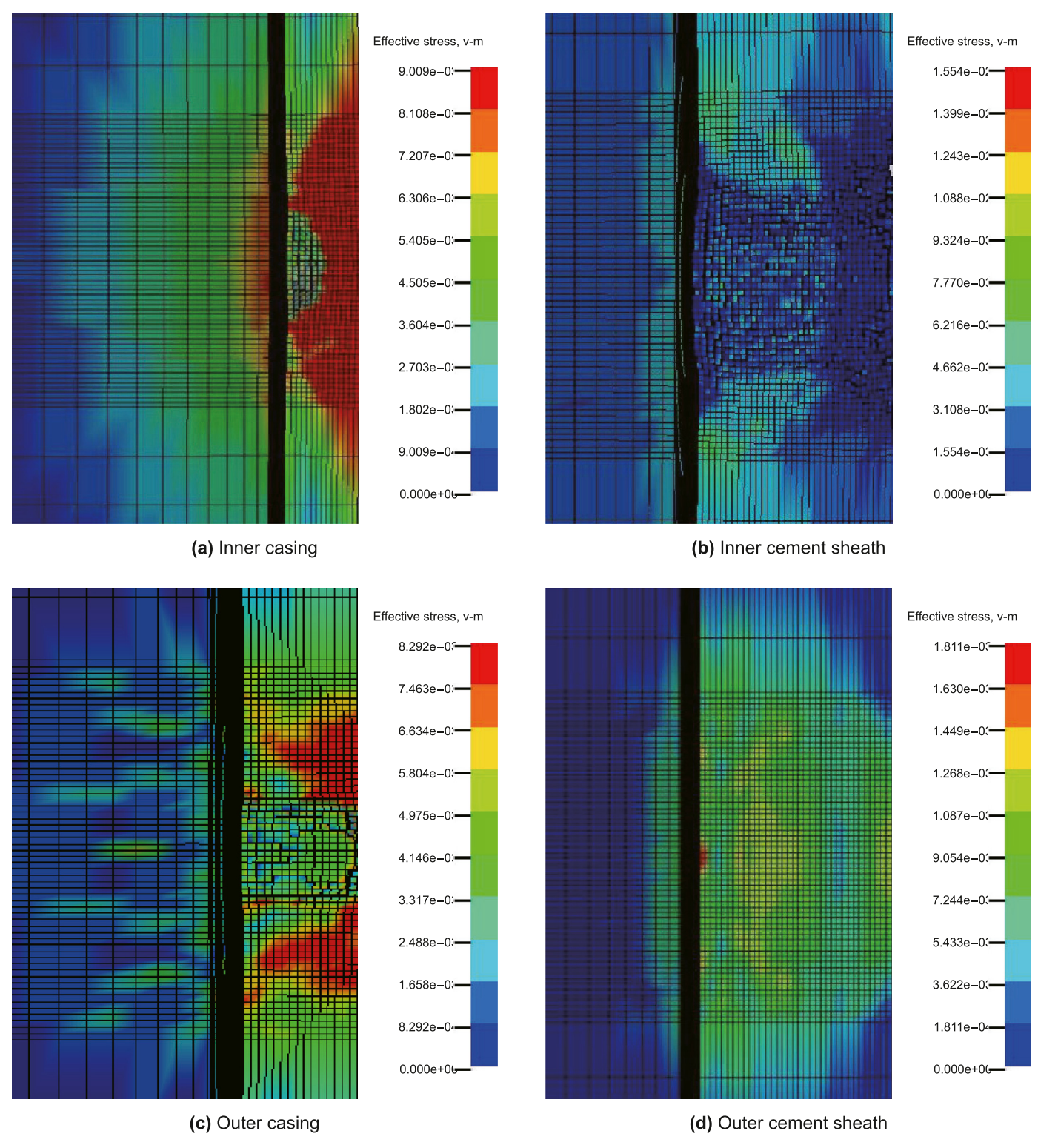


Fig. 3. Cloud map of different model stress distribution at the same time.

optimized analysis of parameters such as shot perforation diameter, perforation density, penetration depth, and phase angle is carried out. Considering the effect of perforation diameter on the extrusion strength of the perforation casing, the critical residual collapsing strength is 40.56 MPa. Referring to Fig. 7(a), the perforation diameter of the outer casing is preferably less than 16.5 mm.

Perforation density is a significant factor affecting well

productivity, especially after penetrating contaminated zones, and the role of perforation density is at the top of all factors. In reservoirs with severe non-homogeneity, the role of perforation density is more significant, and it is generally believed that production also increases with increasing perforation density. However, factors such as the consequent decrease in casing strength are usually neglected, so the upper limit should be constrained (Cheng et al.,

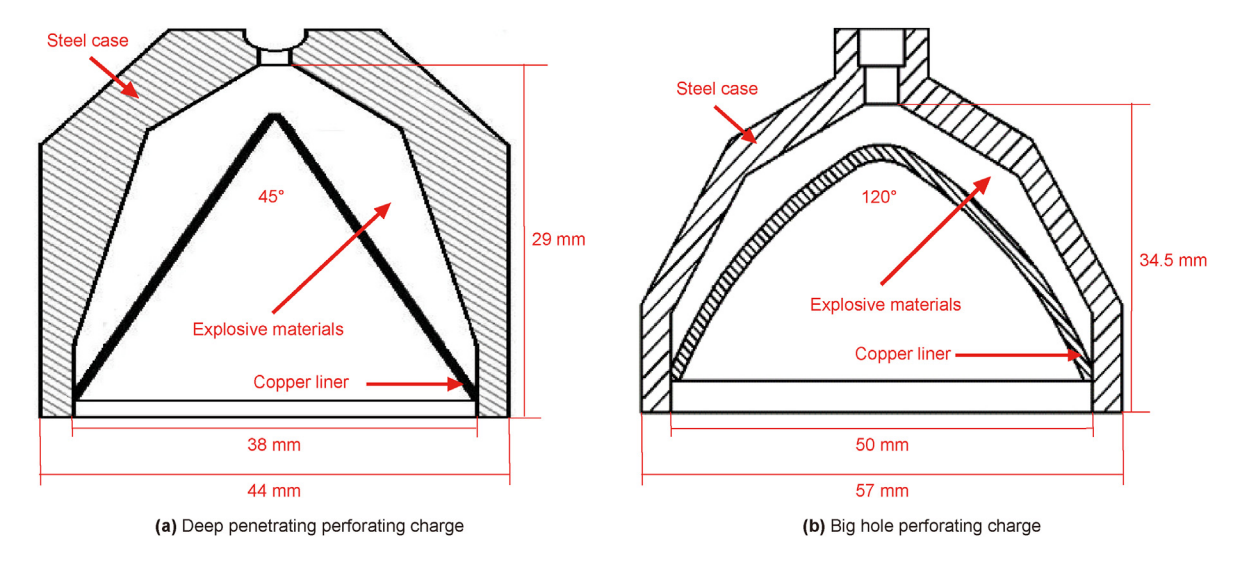


Fig. 4. Perforating charge structure.

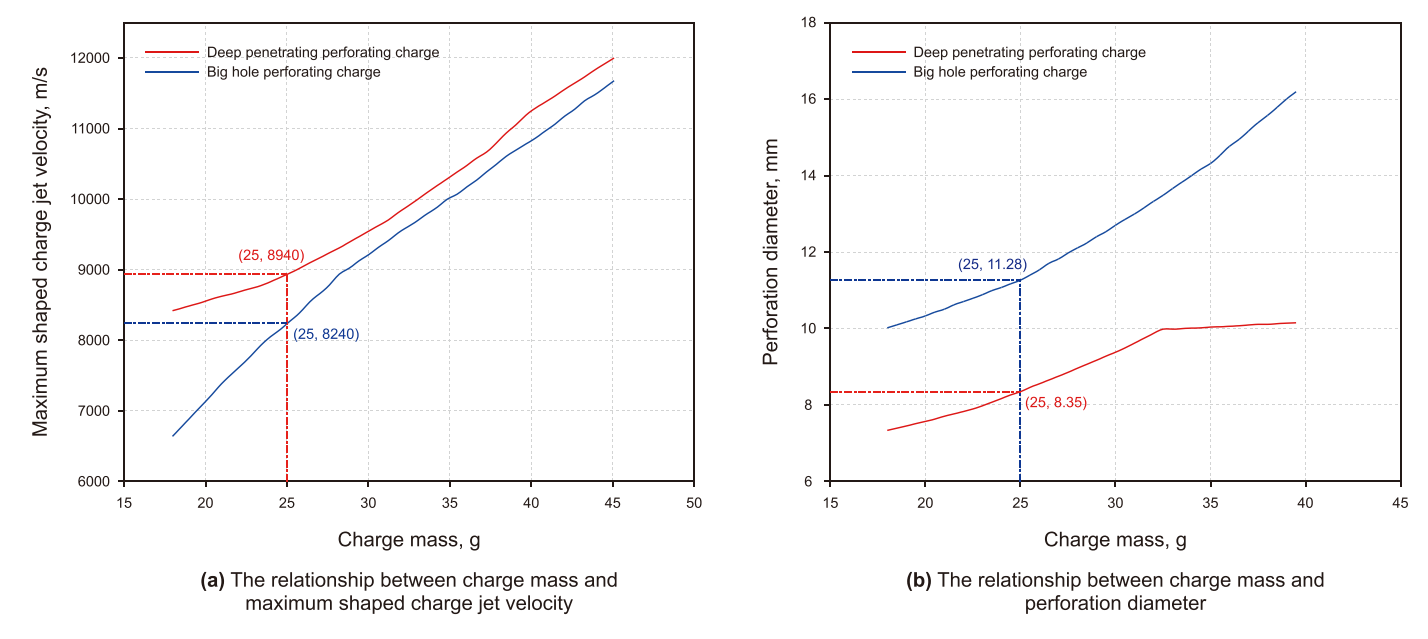


Fig. 5. The influence of charge mass amount of deep penetrating and big hole perforating charge on the maximum shaped charge jet velocity and perforation diameter.

2013; Dou et al., 2019). Considering the effect of perforation density on the extrusion strength of the perforation casing, the perforation density of the outer casing can reach 40 shots/m concerning Fig. 7(b).

114 mm and 127 mm perforating guns can meet the requirements of a double casing perforating process, and will not cause gun explosion, considering the impact of high perforation density on production capacity, it is recommended to use 114 mm gun;

DP perforation charge has better penetrability, the BH perforation charge hole is larger, and the recommended choice of HMX, DP charge, charge mass ≥25 g. In summary, the design can meet the requirements of double casing penetration and safety, the remaining parameters are shown in Table 1.

3. Experimental study of HTHP double-cased perforation in deepwater oil and gas wells

To truly reflect the perforation performance of the shaped

charge penetrating the double casing in a HTHP environment downhole, we design a simplified test of perforation penetrability under high temperature and high-pressure conditions and a fullscale perforation simulation test on the surface at normal temperature and pressure. The former uses a high-temperature and high-pressure test vessel to simulate real perforation conditions in simulated deepwater reservoirs and is a simplified perforation test combining a columnar concrete target with a simulated casing piece to analyze and establish quantitative relationships between perforation depth, perforation diameter, and temperature and pressure. The latter is a multi-group full-scale annular concrete target test conducted under normal temperature and pressure on the ground. The purpose is to study the perforation penetration performance, establish the quantitative relationship between charge mass and perforation depth and perforation diameter, analyze the influence of perforation density on perforation diameter and perforation depth, and carry out research on the influence of different perforation charges on the efficiency of double-cased perforation.

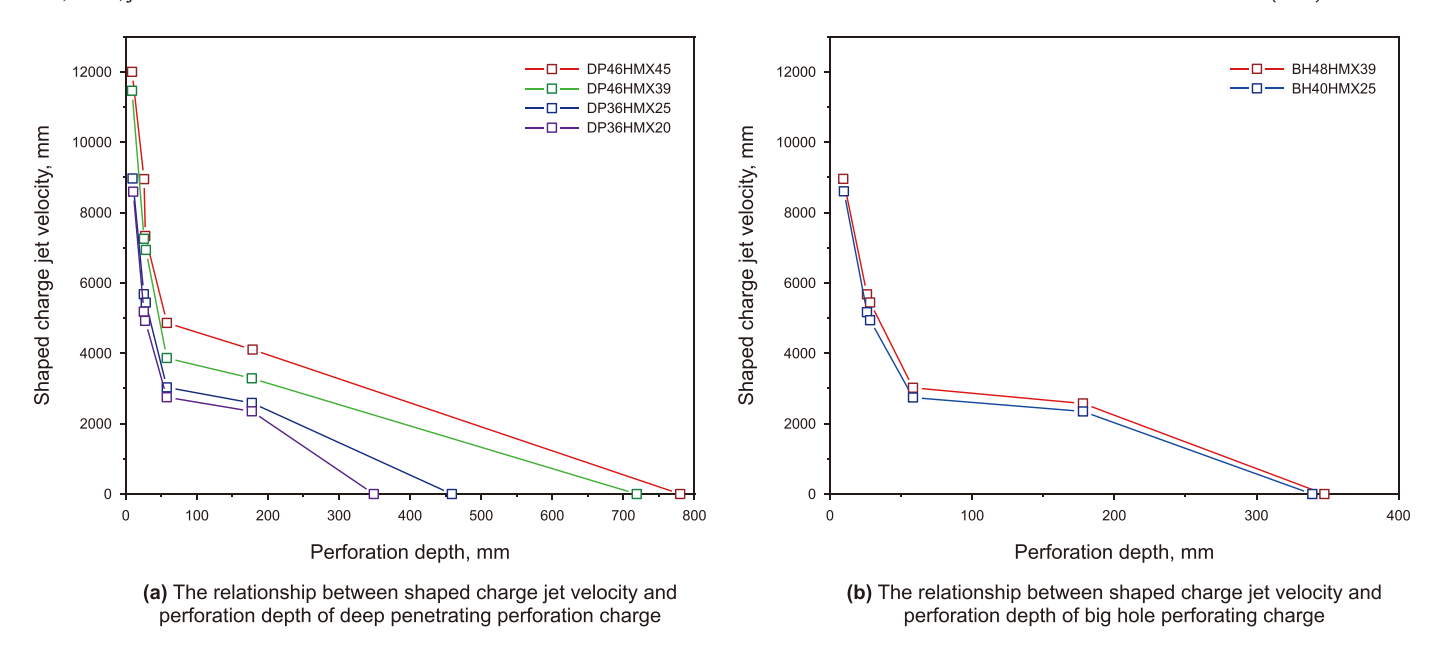


Fig. 6. The influence of charge mass amount of deep penetrating and big hole perforating charge on the shaped charge jet velocity and perforation depth.

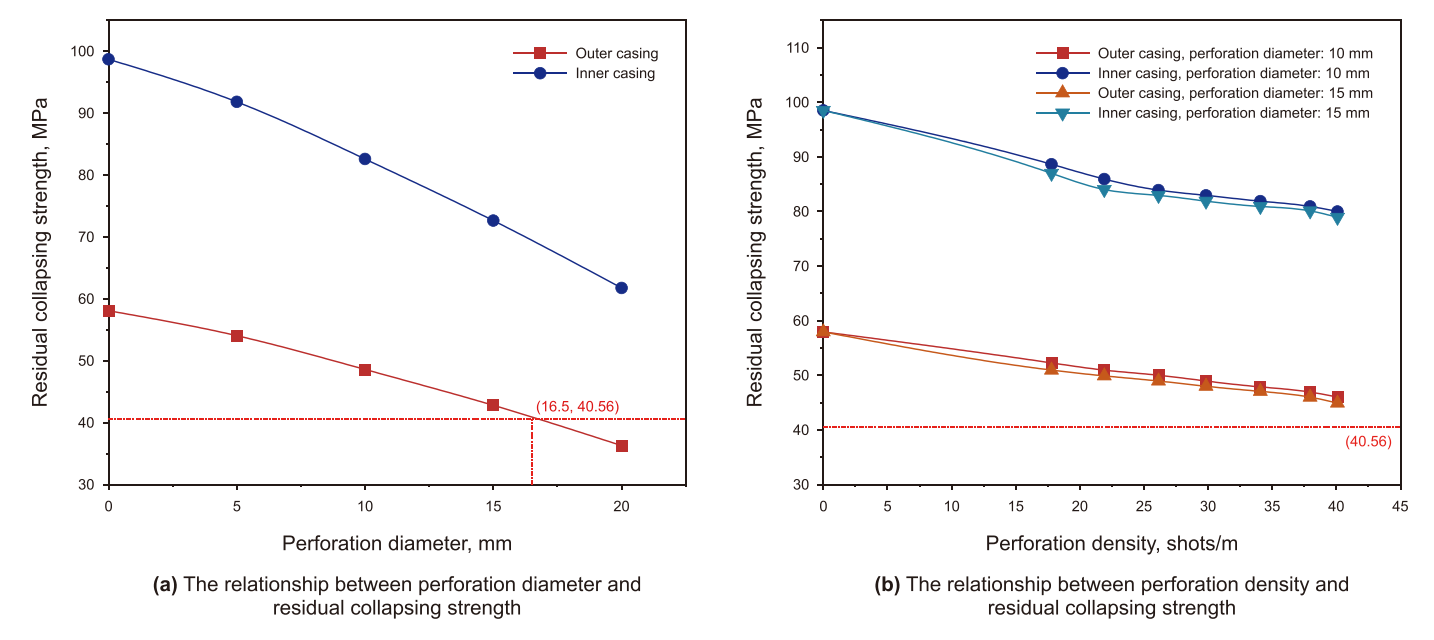


Fig. 7. The influence of perforation diameter and density on the strength of inner and outer casings.

Table 1Optimization of perforation parameter range.

Perforating gun	Perforation density, shots/m	Perforation diameter, mm	Perforation depth, mm	Phase angle, °
127/114 mm	≤40	≤16.5	≥400	0-180

Considering the requirements of perforation density, perforation diameter, perforation depth, and phase angle of the perforation process, the casing and cement sheath materials and parameters used in the design perforation test are consistent with the numerical simulation scheme. We use two types of perforation charges, DP and BH, to conduct tests and develop a reasonable perforation test program that meets the field perforation process concerning the range of perforation parameters optimized by

numerical simulation.

3.1. Double-cased perforation test under high temperature and high-pressure conditions

For the live-fire target test, we make API standard concrete targets according to GB/T 20488-2006 Performance Test Methods for Shaped Perforation Equipment for Oil and Gas Wells and cure





(a) Perforation experiment operation site

(b) Concrete targets

Fig. 8. High temperature and high-pressure perforating charge perforation experiment process.

them for more than 28 days under normal temperature conditions. The average compressive strength is 41.3 MPa and the diameter is 155 mm, of which 10 are 1200 mm in length and 10 are 800 mm in length, totaling 20. The top is prefabricated with simulated casing pieces of the same wall thickness as the casing, the thickness of the gun barrel target piece is 5 mm, the thickness of the inner and outer casing target pieces are 11.51 and 13.84 mm, and the thickness of the inner cement sheath is 19.51 mm.

Three types of perforation charges, DP36HMX25, DP46HMX39, and BH40HMX25, were used to carry out the double casing perforation target testing under the three temperature and pressure conditions of ambient temperature and pressure, 130 °C/44 MPa, and 137 °C/60 MPa in the HTHP generator, taking into consideration the parameters of the equipment used in the HTHP physical experiments in conjunction with the environmental definitions of the HTHP stratum, as shown in Fig. 8.

High-temperature and high-pressure physical experimental equipment assembly is completed, the equipment started to the test predetermined pressure, temperature, and test equipment indicators are as follows: pressure: 145 MPa; temperature: 240 °C; followed by ignition to detonate perforation, to complete the experiment. The condition of the target body and the condition of

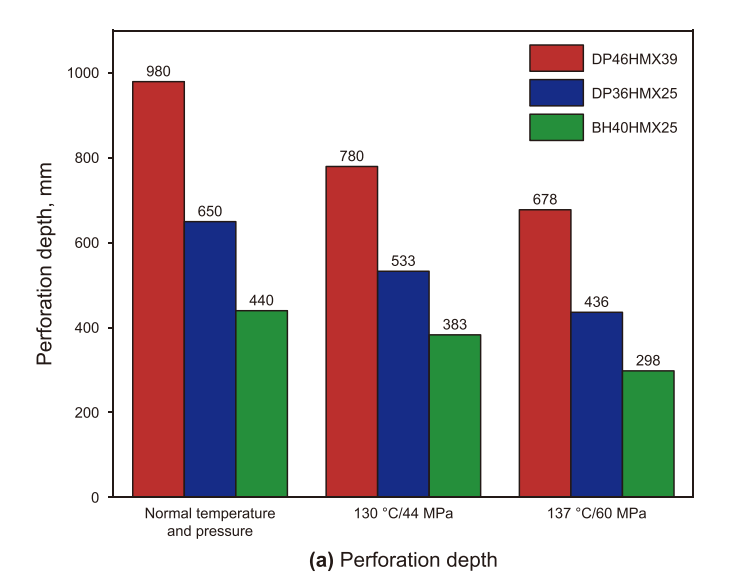
inner and outer casing pieces after perforation are shown in Fig. 9, and perforation depth and perforation diameter on the inner and outer casing are measured.

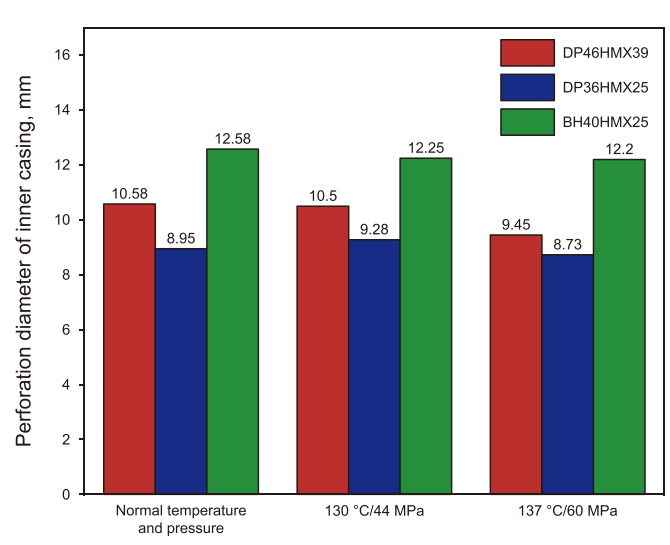
From the comparison graphs of perforation depth and perforation diameter of three different types of perforation charges under different temperature and pressure conditions, as shown in Fig. 10, it can be seen that high temperature and high pressure environments have a more obvious effect on perforation depth and a smaller effect on perforation diameter. The perforation diameter reduction rate of the outer casing is more than 15% higher than that of the inner casing, and the perforation diameter reduction rate of the inner and outer casing will become smaller with the increase of temperature and pressure or the increase of the charge mass, which means that for the DP perforation charge, the perforation charge with high charge mass is beneficial to the double-cased perforation to ensure a certain perforation depth and perforation diameter. The BH perforation charge has a larger perforation diameter reduction rate than the DP perforation charge.

We define the ratio of the loss of perforation depth due to environmental factors to the perforation depth at ambient temperature and pressure as the reduced factor. As shown in Fig. 11, the reduced factors for perforation depth are 0.81, 0.82, and 0.87 at



Fig. 9. Concrete target and casing after the high temperature and pressure experiment.





(b) Perforation diameter of the inner casing

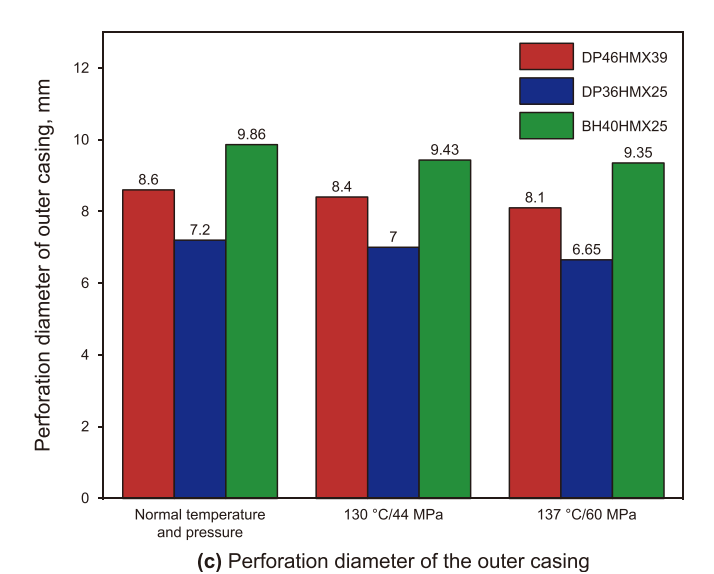


Fig. 10. Comparison of experimental results of different perforating charges under different temperature and pressure conditions.

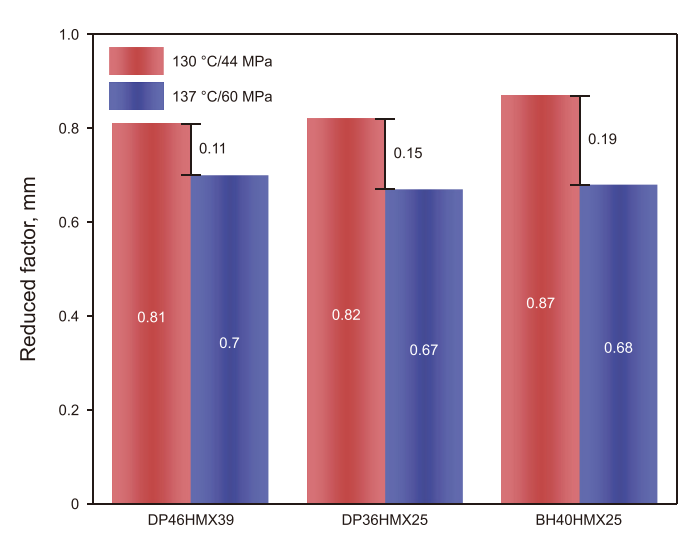


Fig. 11. Comparison of the reduced factor of different perforating charge.

130 °C/44 MPa and 0.70, 0.67, and 0.68 at 137 °C/60 MPa, respectively, compared to the ambient temperature and pressure conditions. With the increase in temperature and pressure, the reduced factor of penetration depth decreases, and the reduced factor of DP perforation charge increases with the decrease in charge mass. It means that high temperature and high pressure have a greater effect on the perforation depth loss of perforation charge with a small charge mass. When the charge mass is the same, the BH perforation charge has a greater reduced factor than the DP perforation charge, and the high temperature and pressure have a relatively large impact on the perforation depth of the BH perforation charge.

3.2. Ground full-scale ring target double-cased perforation test

To study the law of perforation penetrability under normal temperature and pressure conditions, the relationship between charge mass and perforation depth is established, the perforation density is changed, the relationship with perforation diameter and perforation depth is analyzed, and the accuracy of the numerical model is checked. Full-scale tests are conducted under outdoor conditions, with priority given to high-temperature and high-pressure perforation charges and casing matched with perforation guns, uniform perforation/cluster perforation, and mixed loading of different charge intervals.

According to GB/T 20488-2006 Performance Test Methods for Shaped Perforation Equipment of Oil and Gas Wells, API standard full-scale ring concrete target is made, and the ratio of concrete target is cement: sand: water = 1:2:0.52. Maintenance time not less than 28 days, concrete target uni-axial compressive strength not less than 5000 psi, with 2 groups of 2800 mm diameter and 1450 mm height, and 6 groups of 2500 mm diameter and 1450 mm height, a total of 8 groups, refer to Fig. 12. Two sets of casing with a height of 1600 mm are tested by using 114 mm and 127 mm perforation guns: the inner casing has the outer diameter of 177.8 mm and the wall thickness of 11.51 mm; the outer casing has the outer diameter of 244.5 mm and the wall thickness of 13.84 mm. Two sizes of casing are concentrically welded on a bottom surface, and the casing gap is poured with cement paste. Preferred perforation densities: 16, 20, 30, 40 shots/m; phase angle: 90°, 45/135°, 120°; several types of perforation charges, DP36HMX25, DP46HMX39, DP46HMX45, BH48HMX39, and BH40HMX25, are used to carry out ground-based full-scale ring

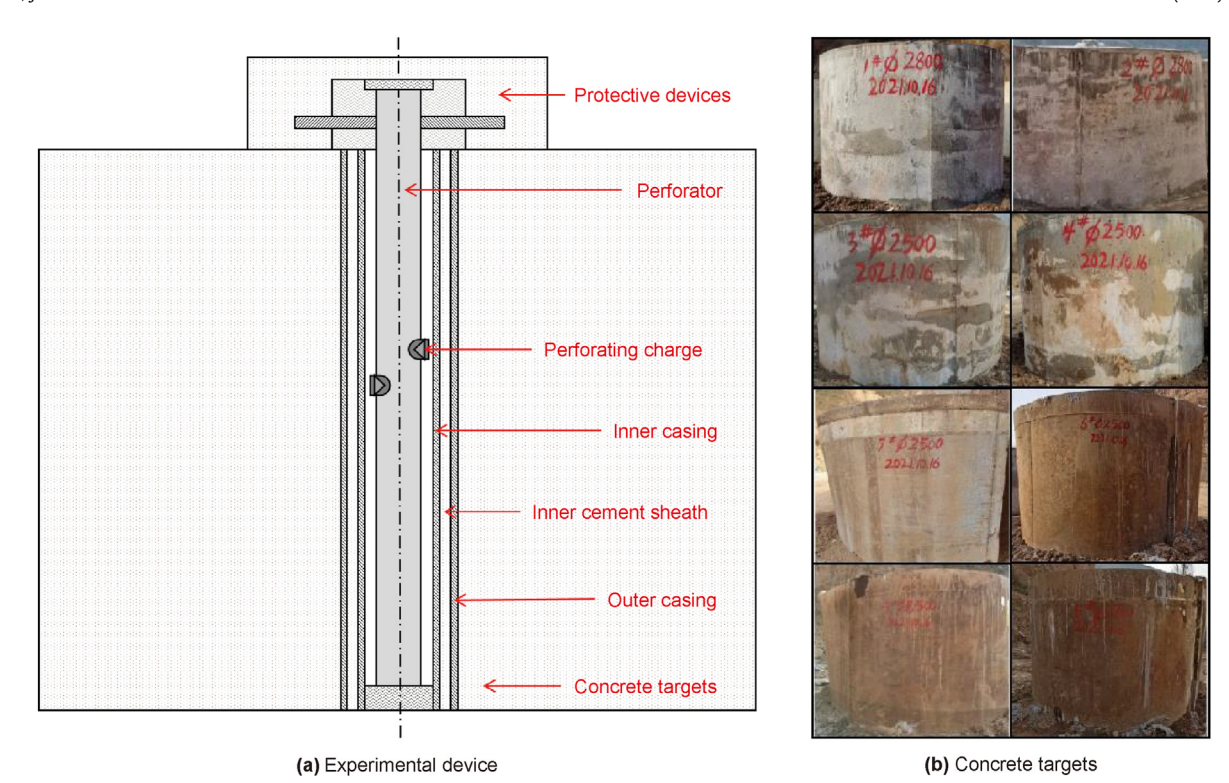


Fig. 12. Full-scale concrete target perforation experiment.



Fig. 13. Perforator and casing.

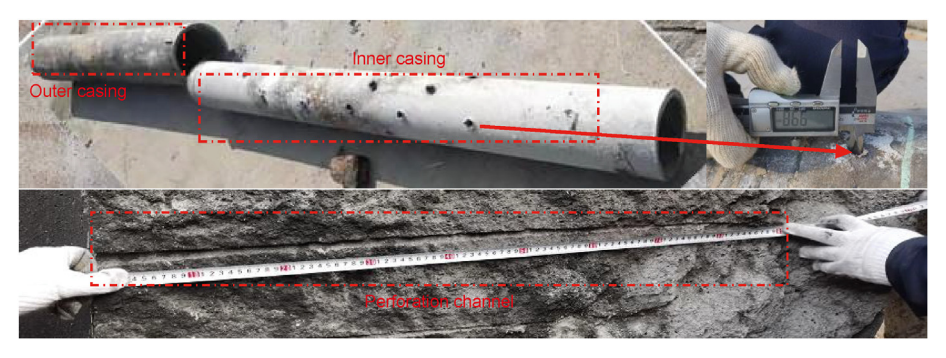


Fig. 14. Concrete target and casing after the full-scale concrete experiment.

target double cased perforation tests.

The assembly of the perforation charge and casing is finished, and the test is started by ignition, as shown in Fig. 13. After the test, the casing is removed and the perforation diameter is observed and measured, as shown in Fig. 14.

To study the law of perforation penetrability under different conditions, and compare the effects of perforation density and charge mass of two types of perforation guns on perforation depth and perforation diameter, referring to Figs. 15 and 16. The simulation results of the eight test programs show that the perforation depth is greater than 400 mm at normal temperature and pressure, and the perforation depth of DP perforation charge is greater than that of BH perforation.

Perforation of the same charge type with different perforation densities: 114 mm perforator with DP36HMX25 charge, with an average perforation depth of 615.0 mm and an average perforation



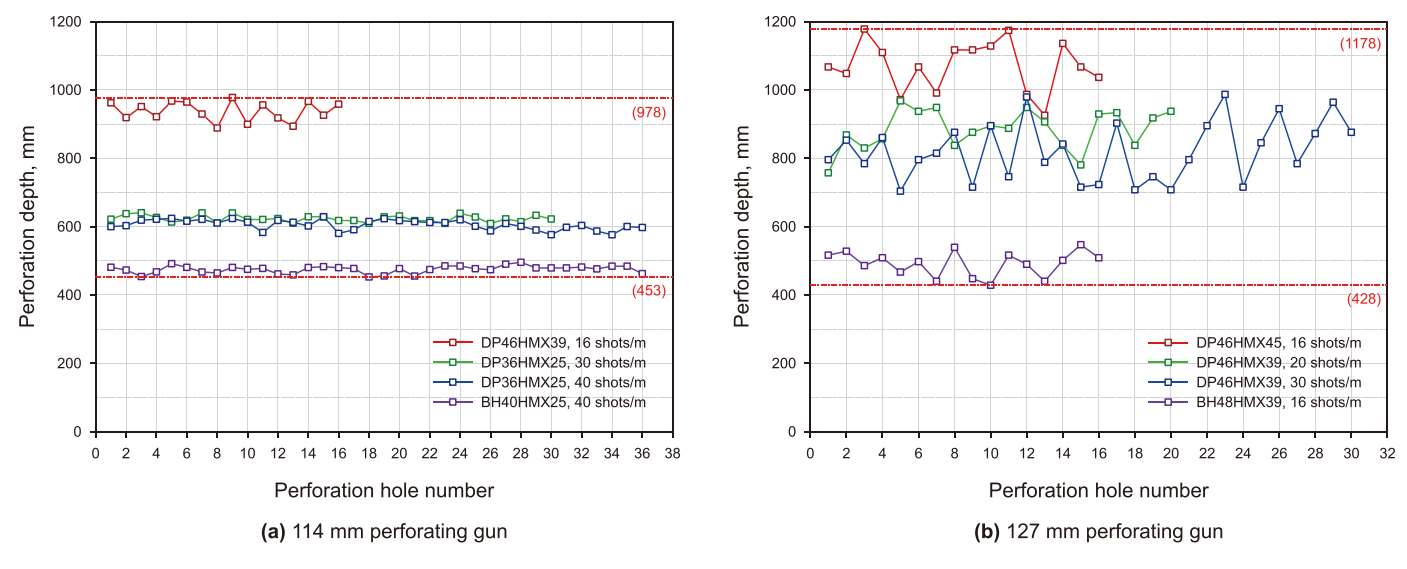


Fig. 15. Perforation depth after the full-scale double casing perforation experiment.

diameter of 8.5 mm at a perforation density of 40 shots/m; The perforation depth at a perforation density of 30 shots/m is 624 mm and the average perforation diameter is 8.0 mm; the perforation depth decreases by 1.4%, and there is a small change in perforation diameter, 127 mm perforator with DP46HMX39 charge, with an average perforation depth of 821 mm and an average perforation diameter of 9.5 mm at a perforation density of 30 shots/m; The perforation depth at a perforation density of 20 shots/m is 882 mm and the average perforation diameter is 9.5 mm, the perforation depth decreases by 6.9%, and the perforation diameter is the same. It shows that in the perforation density range of 16-40 shots/m, when the perforation density increases, there is a slight negative effect on the perforation depth, and the effect on the perforation diameter is extremely small, which is consistent with the numerical simulation, and the perforation density parameter is recommended to be 16 shots/m. With this premise, the average perforation depth of 938.0 mm for 114 mm perforator with DP46HMX39, indicates that the perforation depth increases significantly with the increase of charge mass.

Perforation of different charge types with the same perforation density: under 16 shots/m conditions of 127 mm perforator, the average perforation depth of DP46HMX45 charge is 1068.0 mm and the average perforation diameter is 10.0 mm; The average perforation depth of BH48HMX39 charge is 488.0 mm, and the average perforation diameter is 9.0 mm; the average perforation depth decreases by 54.3%; the average perforation diameter of inner casing of BH48HMX39 charge is 81.8% higher than that of DP46HMX45 charge. Meanwhile, the maximum perforation diameter of the outer casing of the deep perforation charge is 9.38 mm, and the maximum perforation diameter of the outer casing of the big hole charge is 10.1 mm. This indicates that there is a larger increase in inner casing perforation diameter and a smaller increase in outer casing perforation diameter for BH perforation charges than for DP perforation charges.

4. Optimal design of perforation parameters based on numerical simulation and experimental study

Based on the optimized perforation parameters from the numerical simulation of double-cased perforation, a double-cased perforation simulation test was designed for high-temperature and high-pressure service conditions. The results of the normal

temperature and pressure ground full-scale perforation simulation tests are corrected by perforation depth and perforation diameter reduction factors obtained from the simplified tests of perforation penetrability under high temperature and pressure conditions. Based on the law of the quantified effect of different temperature and pressure environments in the wellbore on the perforation efficiency of the double casing and combined with the above experimental correction results, the study verifies the validity of the numerical simulation.

4.1. Correction of test results and comparative analysis

High temperature and high-pressure simulation results show that: compared with normal temperature and pressure conditions, the perforation depth decreases under 130 °C/44 MPa and 137 °C/60 MPa conditions, and the perforation depth decreases more with the increase of temperature and pressure, and the reduced factor is between 0.67 and 0.87. The perforation diameter changes relatively little, and the full-scale simulated test perforation depth is corrected under the actual temperature and pressure conditions according to the reduced factor, referring to Figs. 17 and 18.

The correction results show that the larger the gun diameter, the larger the amount of the charge mass that can be matched and the deeper the hole under a reasonable perforation scheme; the average perforation depth is 717.1 mm when using DP46HMX39 perforation charges and 867.9 mm when using DP46HMX45 at 130 $^{\circ}\text{C}$ and 44 MPa working condition. The average depth of perforation decreased by 21.03% for a 39 g charge mass compared to a 45 g charge mass. The effect of the charge mass on the performance of perforation is relatively large.

Under the same perforation gun, with the increase of perforation density, perforation depth decreases slightly and perforation diameter does not change significantly; Under the working conditions of 130 °C and 44 MPa/137 °C, the average perforation depth of 114 mm perforator with DP36HMX25 charge is 511.5 and 504.5 mm when the perforation density is 30 and 40 shots/m, and the perforation depth decreases by 1.37%, and the effect of perforation density on the performance of 114 mm perforator is relatively small; The average perforation depths of 127 mm perforator with DP46HMX39 charges are 717.1 and 667.5 mm when the perforation density is 20 and 30 shots/m. The perforation depth decreases by 6.92%, and the perforation density has a relatively large impact on

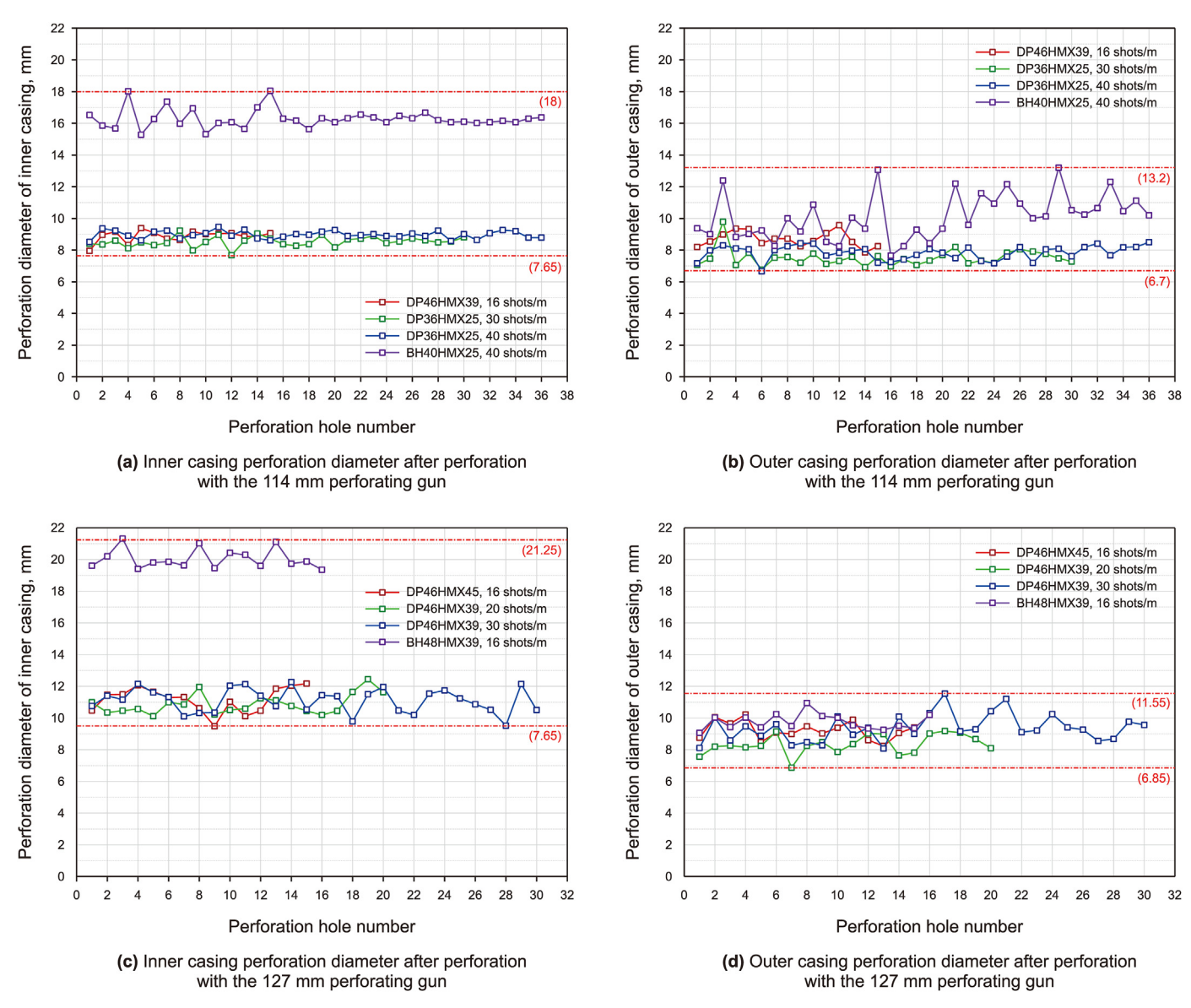


Fig. 16. Perforation diameter after the full-scale double casing perforation experiment.

the performance of the 127 mm perforator.

The greater the amount of charge mass the greater the effect of perforation density on perforation depth. The reduction rate of perforation depth is 1.4% at the two working conditions of 130 °C, 44 MPa/137 °C, and 60 MPa for 114 mm perforator, and that is 6.9% at the same working conditions for 127 mm perforator.

The average perforation depth is 511.5 mm for a 114 mm perforator with DP36HMX25 charge under 130 °C and 44 MPa; The average perforation depth is 399.1 mm for BH40HMX25 charge, and the perforation depth decreases by 21.97%, and the influence of the two perforation charge on the penetration performance is relatively small. The average depth of penetration is 717.1 mm for DP46HMX39 charge under 130 °C and 44 MPa; The average perforation depth is 424.5 mm for BH48HMX39 charge, and the perforation depth decreases by 40.85%, the two types of perforation charge have a relatively large impact on perforation performance. The perforation depth of the DP perforation charge is more than 400 mm, and the perforation depth of the BH perforation charge is always close to or less than 400 mm. Overall, the deep perforation charge is better than the BH perforation charge when using

perforation.

In addition, we corrected and analyzed the long and short axis measurements of the gun body hole, inner casing hole, and outer casing hole for two types of perforators and five types of perforation charge, as shown in Fig. 19.

When different perforations charge, oval holes are basically formed in the gun body, inner casing, and outer casing, but the ratio of the long axis to the short axis is not large, indicating that the shape of the perforation is relatively regular. There is a small difference between the average perforation diameter of high-temperature and high-pressure perforation and the average perforation diameter of normal-temperature and normal-pressure perforation. Overall, the hole size is strongly correlated with the size of the copper liner. Generally, the larger the copper liner, the larger the hole size, and the inner casing perforation diameter increases significantly for BH perforation charge. Under the same copper liner, the perforation diameter also has a certain correlation with the charge mass; generally, the larger the charge mass, the larger the hole size.

The results of the numerical simulation of double-cased

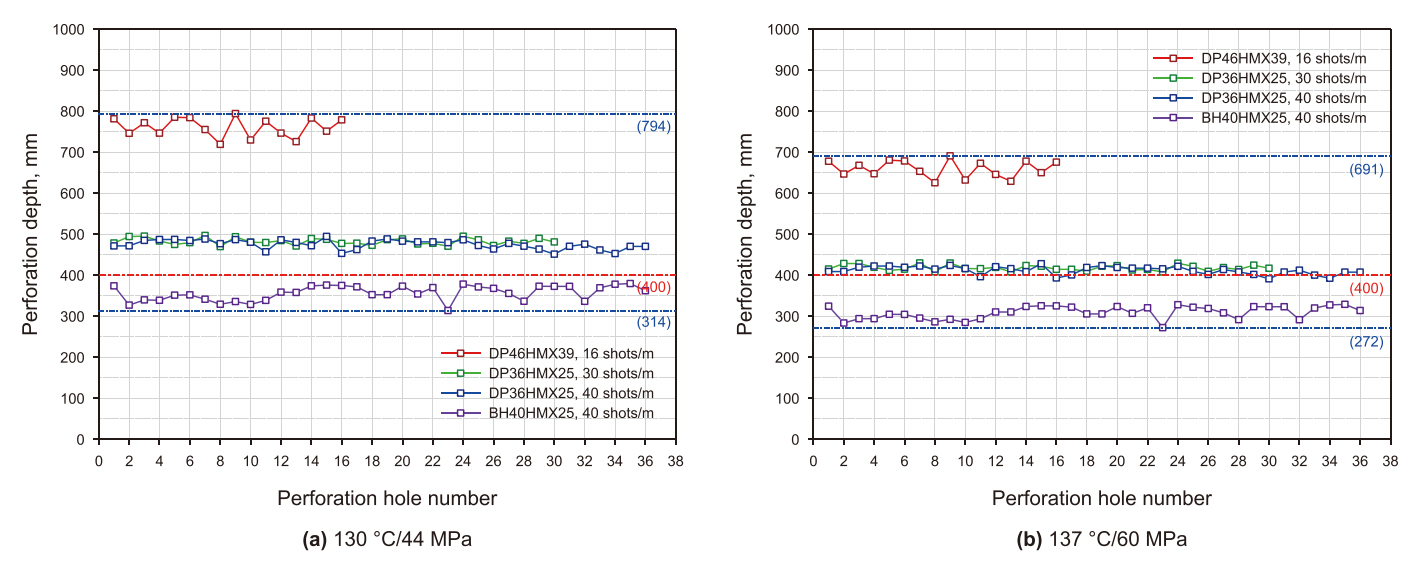


Fig. 17. Correction results of perforation depth for full-scale double casing perforation experiment of 114 mm perforating gun.

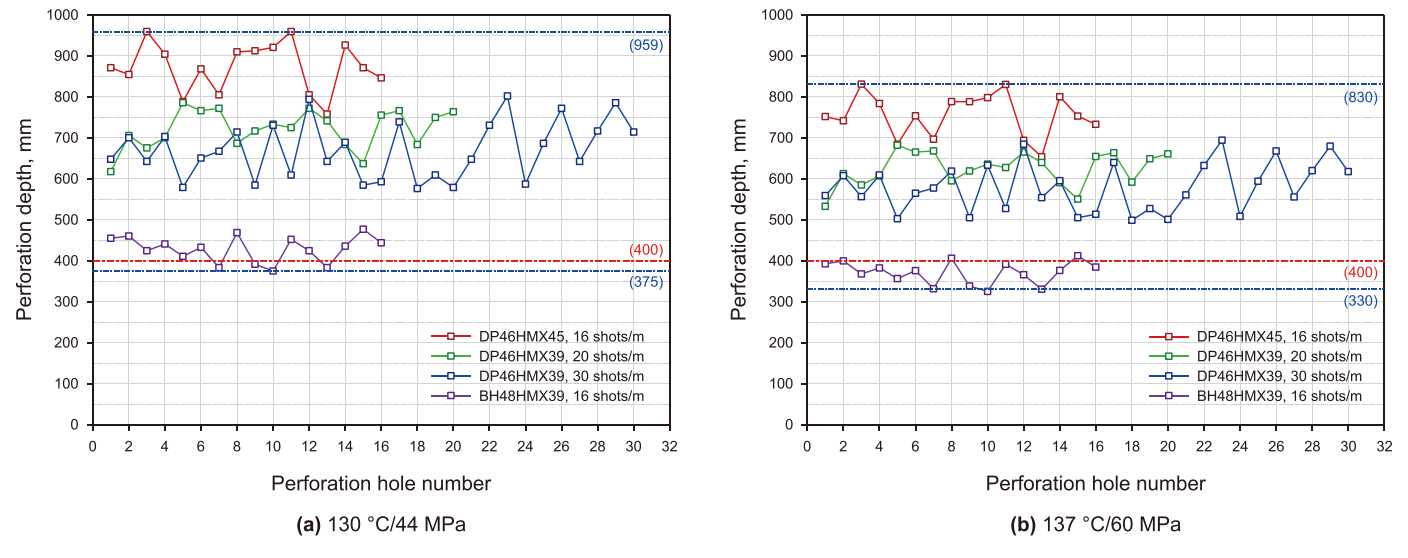


Fig. 18. Correction results of perforation depth for full-scale double casing perforation experiment of 127 mm perforating gun.

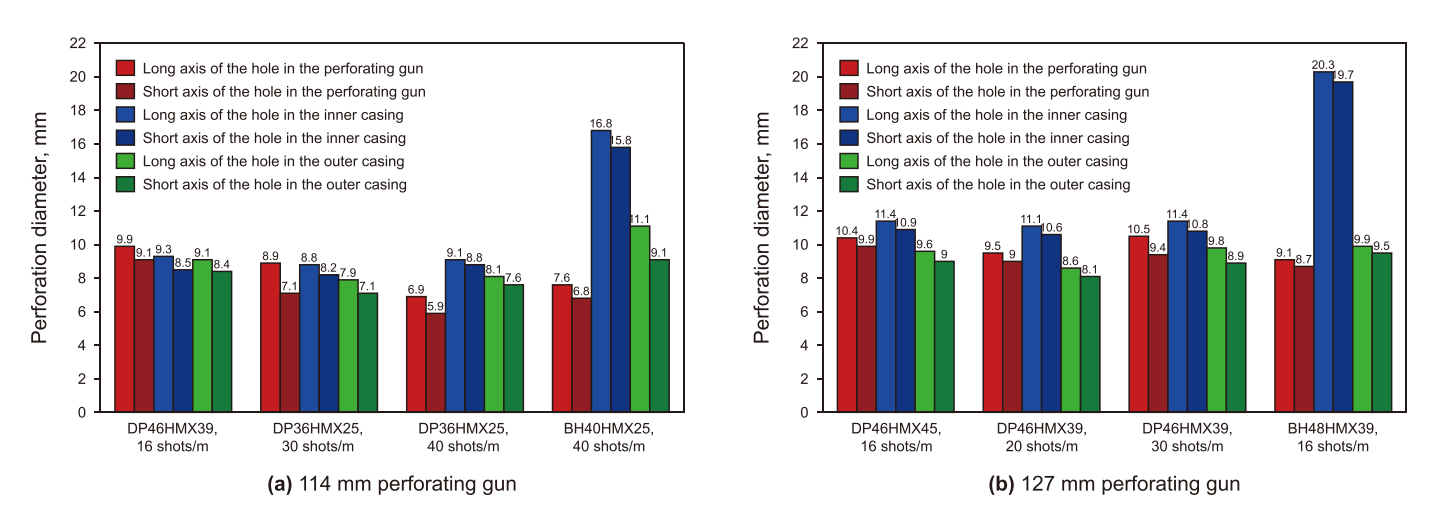


Fig. 19. Correction results of perforation diameter for full-scale double casing perforation experiment.

Table 2Comparison between numerical simulation results of 137 °C/60 MPa double casing perforation and full-scale experiment correction results of 114 mm perforating gun.

Perforator	114 mm	114 mm				
Perforation charge		DP46HMX39	DP36HMX25	DP36HMX25	BH40HMX25	
Perforation density, shots/m		16	30	40	40	
Phase angle, °		90	45/135	45/135	45/135	
Perforation diameter of the inner casing, mm	Test	8.93	8.54	8.98	16.3	
	Simulation	9.23	8.78	8.65	15.9	
Perforation diameter of the outer casing, mm	Test	8.72	7.50	7.73	10.11	
	Simulation	9.15	7.82	7.88	13.5	
Perforation depth of the concrete targets, mm	Test	661	419	413	311	
	Simulation	720	460	430	340	

Table 3Comparison between numerical simulation results of 137 °C/60 MPa double casing perforation and full-scale experiment correction results of 127 mm perforating gun.

Perforator	127 mm				
Perforation charge		DP46HMX45	DP46HMX39	DP46HMX39	BH48HMX39
Perforation density, shots/m		16	20	30	16
Phase angle, °		90	120	120	90
Perforation diameter of the inner casing, mm	Test	11.16	10.83	11.11	20.01
	Simulation	11.3	11.1	11.3	20.8
Perforation diameter of the outer casing, mm	Test	9.28	8.32	9.38	9.73
•	Simulation	9.0	8.64	9.0	9.4
Perforation depth of the concrete targets, mm	Test	752	621	578	330
	Simulation	780	630	610	348

perforation at 137 °C/60 MPa are compared with the results of full-scale test correction, as shown in Tables 2 and 3.

Based on the ground full-scale simulation test of double-cased perforation, we checked the accuracy of numerical simulation results under the formation temperature and pressure conditions, and the accuracy of numerical simulation results was verified by the test results. The maximum error of the average perforation depth does not exceed 8.91%, and the maximum error of the average perforation diameter does not exceed 4.7%, which is small, and the accuracy of the simulation calculation is within the acceptable range. Referring to the constraint range of perforation parameters proposed by the dynamic simulation, combined with the above analysis, the high temperature and high-pressure conditions have a large negative impact on the perforation effect of small charge mass and BH perforation charge. It is recommended to use the combination of perforation parameters such as a 114 mm perforator, DP36HMX25 charge, perforation density of 40 shots/m, phase angle of 45/135°, perforation depth of 413 mm, perforation diameter of 7.73 mm, etc., which can get the best perforation effect of the double casing.

The above experimental results verify the accuracy of the numerical simulation results, and both numerical simulation and experimental results indicate that it is feasible to use double-cased perforation with DP perforation charge.

5. Conclusion

(1) A double-cased perforation dynamic simulation model including explosive materials, copper liner, perforation fluid, steel case, and casing was established to determine the quantitative relationship between the charge amount, charge mass, perforation depth, and perforation diameter. When the charge mass is greater than 25 g and the muzzle velocity is greater than 8000 m/s, the velocity of perforating charge leaving the outer casing can be ensured to be greater than 850 m/s. The deep penetration distance of the DP perforation charge is also more than 400 mm, which

establishes the critical condition of the perforation penetration of the double casing.

- (2) Based on the simulation calculation of double-cased perforation with DP and BH perforation charges suitable for deepwater HTHP reservoirs, the influencing factors of perforation depth and perforation diameter and the strength of the inner and outer casing are analyzed. On the premise of satisfying the penetration and safety of double-layer casing, the constrained range of perforating parameters of double-layer casing was proposed: Considering the influence of perforation diameter and depth on the residual collapsing strength of perforated casing, it is recommended that the perforation diameter of the outer casing be less than 16.5 mm and the casing density be less than 40 shots/m because the critical residual extrusion strength is 40.56 MPa.
- (3) We designed a double-cased perforation test to simulate the HTHP environment of the reservoir. Compared with normal temperature and pressure conditions, HTHP has a greater influence on the perforation depth but little influence on the diameter. Under the condition of 130 °C/44 MPa, the reduction coefficient of perforating depth for three different types of perforating charges is 0.81–0.87. Under the working condition of 137 °C/60 MPa, the reduction coefficient of perforating depth for three different types of perforating charges is 0.67–0.70. The perforation diameter reduction rate of the outer casing is more than 15% compared with that of the inner casing. The results of full-scale perforation simulation tests at ambient temperature and pressure on the ground were corrected using the scientific technical data obtained for the reduced factor.
- (4) According to the constrained range of perforating parameters proposed by dynamic perforating simulation and the analysis of double-layer casing perforating tests in an HTHP environment, the optimal combination of perforating parameters is proposed: DP36HMX25 perforating charge is adopted, with a perforation density of 40 shots/m, a phase of 45/135°, the penetration depth is greater than 400 mm, the aperture is greater than 7 mm, etc.

(5) The research will be of great significance to the development of special oil and gas reservoirs with harsh working conditions such as deep wells, collapse-prone, sand-prone, HTHP, formation slippage, or salt-paste layer creep. Based on the existing foundation in this paper, the completion mode of double casing or multi-layer casing can be further studied.

Data availability statements

All data, models, and code generated or used during the study appear in the submitted paper.

CRediT authorship contribution statement

Gang Bi: Writing — review & editing, Writing — original draft, Supervision, Software, Resources, Methodology, Investigation. **Fei Han:** Writing — review & editing, Writing — original draft, Software, Investigation. **Jie-Min Wu:** Writing — original draft, Investigation. **Pei-Jie Yuan:** Writing — original draft, Investigation. **Shuai-Shuai Fu:** Investigation. **Ying Ma:** Investigation.

Declaration of competing interest

The authors declared that they have no conflicts of interest to this work.We declare that we do not have any commercial or associative interest that represents a conflict of interest in connection with the work submitted.

Acknowledgement

The authors gratefully acknowledge the support of the Foundation of Natural Science Foundation of Shaanxi Province, Grant/Award nos. 2023-JC-YB-361 and National Natural Science Foundation (Number 52104033).

References

Chen, Y., Xu, J., Jia, L.X., et al., 2018. Casing selection for thermal wells under condition of thermal strength attenuation and high temperature corrosion in

- offshore oilfield. Surf. Technol. 47 (2), 195–201. https://doi.org/10.16490/i.cnki.issn.1001-3660.2018.02.031.
- Cheng, L.S., Luo, Y.Y., Ding, Z.P., 2013. Fuzzy comprehensive evaluation model for estimating casing damage in heavy oil reservoir. Petrol. Sci. Technol. 31 (10), 1092–1098. https://doi.org/10.1080/10916466.2010.536802.
- Deng, Q., Zhang, H., Li, J., et al., 2019. Study of downhole shock loads for ultra-deep well perforation and optimization measures. Energies 12 (14), 1–23. https://doi.org/10.3390/en12142743.
- Dong, K.X., Li, Q.E., Liu, W., et al., 2021. Optimization of perforation parameters for horizontal wells in shale reservoir. Energy Rep. 7 (S7), 1121–1130. https:// doi.org/10.1016/I.EGYR.2021.09.157.
- Dou, Y.H., Cao, Y.P., Li, M.F., et al., 2019. Experimental and theoretical study on the mechanical characteristics of perforated casings. Procedia Struct. Integr. 22 (C), 33–42. https://doi.org/10.1016/j.prostr.2020.01.005.
- Dou, Y.H., Yan, R., Li, M.F., 2016. Optimization of perforating parameter for high pressure fracturing well based on finite element analysis, 25 (1), 1–3. https://doi.org/10.3969/i.issn.1004-4388.2016.01.001.
- Hu, F., Wu, H., Fang, Q., et al., 2017. Impact performance of explosively formed projectile (EFP) into concrete targets. Int. J. Impact Eng. 109, 150–166. https://doi.org/10.1016/j.ijimpeng.2017.06.010.
- Hu, J.C., Xu, J.P., Wang, S.Z., et al., 2014. An optimal model for predicting the productivity of perforated vertical HTHP wells. Can. J. Chem. Eng. 92 (7), 1247–1259. https://doi.org/10.1002/cjce.21970.
- Kong, C.Y., Zhang, D.R., Liang, Z., et al., 2017. Mechanical analysis of drill bit during dual-casing sidetracking. J. Petrol. Sci. Eng. 159, 970–976. https://doi.org/ 10.1016/j.petrol.2017.09.040.
- Li, J., Xu, J., Wang, K.J., et al., 2019. New optimization design method for perforation parameter based on optimal perforation depth analysis. J. SW Petrol. Univ. (Sci. Technol. Ed.) 41 (5), 142–149. https://doi.org/10.11885/j.issn.1674-5086.2018.09.12.02.
- Liu, X.B., Li, J., Yang, H.W., et al., 2022. A new investigation on optimization of perforation key parameters based on physical experiment and numerical simulation. Energy Rep. 8, 13997–14008. https://doi.org/10.1016/
- Luo, X.B., Jiang, L.F., Su, Y.C., et al., 2015. The productivity calculation model of perforated horizontal well and optimization of inflow profile. Petroleum 1 (2), 154–157. https://doi.org/10.1016/j.petlm.2015.04.002.
- Wang, W., Li, J., Zhang, Q.L., et al., 2018. Optimal design on the perforation parameters of medium and deep reservoirs in Bohai Oilfield. Oil Drill Prod. Technol. 40, 150–153. https://doi.org/10.13639/j.odpt.2018.S0.042.
- Wang, X.H., Tang, M.R., Du, X.F., et al., 2022. Three-dimensional experimental and numerical investigations on fracture initiation and propagation for oriented limited-entry perforation and helical perforation. Rock Mech. Rock Eng. 56 (1), 437–462. https://doi.org/10.1007/S00603-022-03069-2.
- Xing, X.S., Qiu, H., Wen, M., et al., 2022. Numerical simulation investigation of perforation parameter optimization design based on orthogonal experimental method. Sci. Technol. Eng. 22 (25), 10952–10957. https://doi.org/10.3969/ j.issn.1671-1815.2022.25.015.
- Zhao, X.L., Zhao, Y.Z., Wang, Z.L., et al., 2021. Wellbore temperature distribution during drilling of natural gas hydrate formation in South China sea. Petroleum 7 (4), 451–459. https://doi.org/10.1016/J.PETLM.2021.10.008.